

## Nonequilibrium quantum fields from first principles

Jürgen Berges and Szabolcs Borsányi

Universität Heidelberg, Institut für Theoretische Physik,  
Philosophenweg 16, 69120 Heidelberg, Germany

*Received 1 December 2005*

**Abstract.** Calculations of nonequilibrium processes become increasingly feasible in quantum field theory from first principles. There has been important progress in our analytical understanding based on 2PI generating functionals. In addition, for the first time direct lattice simulations based on stochastic quantization techniques have been achieved. The quantitative descriptions of characteristic far-from-equilibrium time scales and thermal equilibration in quantum field theory point out new phenomena such as prethermalization. They determine the range of validity of standard transport or semi-classical approaches, on which most of our ideas about nonequilibrium dynamics were based so far. These are crucial ingredients to understand important phenomena in high-energy physics related to collision experiments of heavy nuclei, early universe cosmology and complex many-body systems.

*Keywords:* nonequilibrium, 2PI effective action, lattice simulations

*PACS:* 11.10.Wx, 12.38.Mh, 05.70.Ln

### 1. Characteristic far-from-equilibrium time scales

Understanding the dynamics of quantum fields far away from the ground state or thermal equilibrium is a challenge touching many aspects of physics, ranging from early cosmology or collision experiments with heavy nuclei to ultracold quantum gases in the laboratory. One of the most crucial aspects concerns the characteristic time scales on which thermal equilibrium is approached. Much of the recent interest derives from observations in collision experiments of heavy nuclei at RHIC. The experiments seem to indicate the early validity of hydrodynamics after somewhat less than 1 fm, whereas the present theoretical understanding of QCD suggests a longer thermal equilibration time.

Here it is important to note that different quantities effectively thermalize on different time scales and a complete thermalization of all quantities may not be

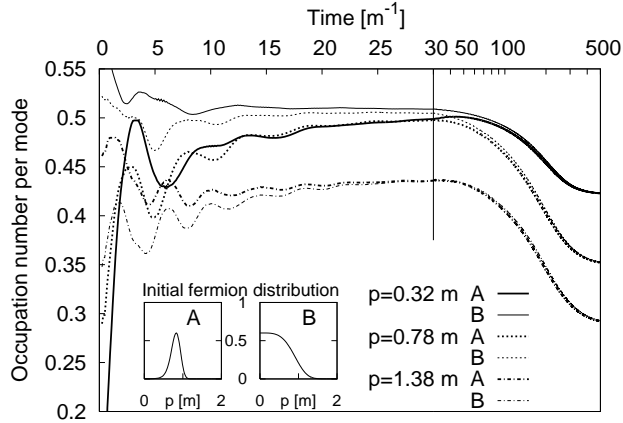


**Fig. 1.** Fermion occupation number for three different momentum modes as a function of time in the chiral quark meson model of Ref. [ 1].

necessary to explain the observations. This has been pointed out in Ref. [ 1], where it was shown for a chiral quark-meson model that the prethermalization of important observables occurs on time scales dramatically shorter than the thermal equilibration time. As an example, Fig. 1 shows the nonequilibrium time evolution of fermion occupation number for three different momentum modes in this model. The evolution is given for two different initial particle number distributions A and B shown in the insets, with *same* energy density. Therefore, both runs have to lead to the same distributions in thermal equilibrium. The vertical line in Fig. 1 marks the characteristic time scale  $\sim t_{\text{damp}}$ , after which the details about the initial distributions A or B are effectively lost. One observes that this happens far before the late-time approach to thermal equilibrium. The time  $t_{\text{damp}}$  for the effective loss of initial condition details is an important characteristic time scale in nonequilibrium dynamics, which is very different from the thermal equilibration time  $t_{\text{eq}}$ . Note that the long-time behavior to thermal equilibrium is shown on a logarithmic scale in Fig. 1 (in units of the scalar thermal mass  $m$ ).

In contrast to the very long time  $t_{\text{eq}}$  for complete thermal equilibration, prethermalization of the (average) equation of state sets in extremely rapidly on a time scale

$$t_{\text{pt}} \ll t_{\text{damp}} \ll t_{\text{eq}}. \quad (1)$$

In Fig. 2 we show the ratio of average pressure (trace over space-like components of the energy-momentum tensor) over energy density,  $w = p/\epsilon$ , as a function of time. One observes that an almost time-independent equation of state builds up very early, even though the system is still far from equilibrium! Here the prethermalization time  $t_{\text{pt}}$  is of the order of the characteristic inverse mass scale  $m^{-1}$ . This is a typical consequence of the loss of phase information by summing over oscillating functions with a sufficiently dense frequency spectrum. If the “temperature” ( $T$ ), i.e. average

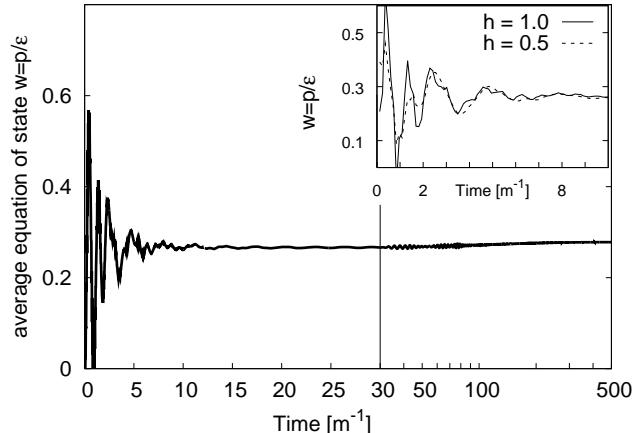


**Fig. 2.** The ratio of average pressure over energy density  $w$  as a function of time. The inset shows the early stages for two different couplings  $h$  and demonstrates that the prethermalization time is rather independent of the interaction details.

kinetic energy per mode, sets the relevant scale one finds  $T t_{\text{pt}} \simeq 2 - 2.5$  [ 1]. For  $T \gtrsim 400 - 500$  MeV one obtains a very short prethermalization time  $t_{\text{pt}}$  of somewhat less than 1 fm.

This is consistent with very early hydrodynamic behavior, however, it is not sufficient as noted in Refs. [ 1, 2]. Beyond the average equation of state, a crucial ingredient for the applicability of hydrodynamics for collision experiments [ 3] is the approximate isotropy of the local pressure. More precisely, the diagonal (space-like) components of the local energy-momentum tensor have to be approximately equal. Of particular importance is the possible isotropization far from equilibrium. The relevant time scale for the early validity of hydrodynamics could then be set by the isotropization time. The analysis of simple models lead to an isotropization time which is given by the characteristic damping time  $\sim t_{\text{damp}}$  (cf. Figs. 1) [ 4]. However, a possible weak-coupling mechanism for faster isotropization in gauge theories such as QCD has been identified in Ref. [ 2] in terms of plasma instabilities [ 5]. Whether this can explain the experimental observations or whether they suggest that we have to deal with some new form of a “strongly coupled Quark Gluon Plasma” is an important open question.

## 2. What can we learn from transport or kinetic theory?

For out-of-equilibrium calculations there are additional complications, which do not appear in thermal equilibrium or vacuum. Standard approximation techniques, such as perturbation theory, are not uniform in time and fail to describe thermalization. Aspects of systems with high occupation numbers are often successfully described using classical field theory methods. However, classical Rayleigh-Jeans divergences

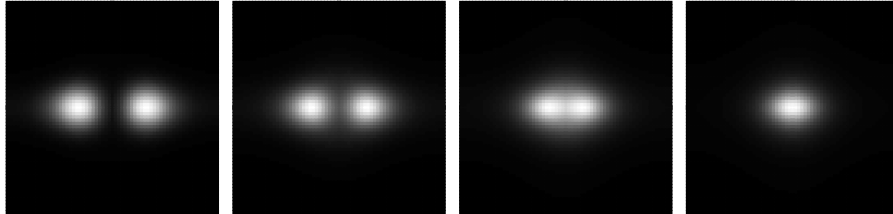


**Fig. 3.** Snapshots at times  $t \simeq 0$ ,  $t_{\text{damp}}/2$ ,  $t_{\text{damp}}$  and  $3t_{\text{damp}}/2$  of the initially anisotropic occupation number distribution as a function of  $p_{\perp}$  (vertical) and  $p_{\parallel}$  (horizontal). The shown resolution was achieved by using a  $64^3$  spatial lattice.

and the lack of genuine quantum effects — such as the approach to quantum thermal equilibrium characterized by Bose-Einstein or Fermi-Dirac statistics — limit their use.

Most theoretical approaches to the important question of thermalization have been limited to semi-classical systems in the weak-coupling limit so far. With the advent of new computational techniques a more direct account of quantum field degrees of freedom becomes more and more possible. There has been important progress in our understanding of nonequilibrium quantum fields using suitable resummation techniques based on 2PI generating functionals [ 6]. They have led to quantitative descriptions of far-from-equilibrium dynamics and thermalization in a variety of scalar and fermionic quantum field theories so far. An example for the results of such a first-principles calculation within a quark-meson model in 3+1 dimensions is given in Figs. 1 and 2. One important application of these quantum field theoretical 2PI methods is to test standard transport or semi-classical approaches, on which most of our ideas about nonequilibrium dynamics are based so far.

Several of these tests have been done for simple scalar  $\lambda\Phi^4$  quantum field theories for not too strong couplings  $\lambda$ , which are well under quantitative control using 2PI techniques. Following Ref. [ 4], we consider a class of anisotropic initial conditions with an initially high occupation number of modes moving in a narrow momentum range around the “beam direction”  $p_3 \equiv p_{\parallel} = \pm p_{\text{ts}}$ . The spatially homogeneous occupation numbers for modes with momenta perpendicular to this direction,  $p_1^2 + p_2^2 \equiv p_{\perp}^2$ , are small or vanishing. The situation is reminiscent of some aspects of the anisotropic initial stage in the central region of two colliding wave packets.<sup>1</sup> Of course, a peaked initial particle number distribution is not very specific and is thought to exhibit characteristic properties of nonequilibrium dynamics for a large variety of physical situations.

An example of the earlier stages of such an evolution is shown in Fig. 3. Shown are snapshots of the occupation number distribution as a function of  $p_{\perp}$  (vertical) and  $p_{\parallel}$  (horizontal), where bright (dark) regions correspond to high (low) occupation numbers. The initial Gaussian distribution is centered around a momentum of the

<sup>1</sup>Other interesting scenarios include “color-glass”-type initial conditions with distributions  $\sim \exp(-\sqrt{p_{\perp}^2}/Q_s)$  peaked around  $p_3 = 0$  with “saturation” momentum  $Q_s$ .

order of the renormalized thermal mass, and we will consider amplitudes of order one for the comparisons below (see [4] for details). From Fig. 3 it can be seen that after the characteristic damping time  $t_{\text{damp}}$  the distribution starts to become rather independent of the momentum direction. Finally, at about  $3t_{\text{damp}}/2$  the figure shows an almost perfectly isotropic situation. We emphasize that the distribution is still far from equilibrium. The situation is similar to what is displayed in Fig. 1, where the vertical line indicates about  $t_{\text{damp}}$ . In general, we find that the characteristic damping time is well described by the standard relaxation-time approximation

$$t_{\text{damp}} \simeq -\frac{2\omega^{(\text{eq})}}{\tilde{\Sigma}_\rho^{(\text{eq})}} \simeq \frac{4\pi m}{3\lambda^2 T^2}, \quad (2)$$

where the imaginary part of the thermal equilibrium self-energy  $-\tilde{\Sigma}_\rho^{(\text{eq})}/2$  in Fourier-space is evaluated for on-shell frequency  $\omega^{(\text{eq})}$  for momentum  $p_{\text{ts}}$ . The second equality in (2) is only valid for sufficiently high temperatures and weak couplings. We emphasize that the relaxation-time approximation (2) does not describe the thermalization time  $t_{\text{eq}}$  [4].

The question is whether transport or kinetic equations can be used to quantitatively describe the early-time behavior  $t < t_{\text{damp}}$ , which is necessary if their application to the problem of fast apparent thermalization explained in Sec. 1 is viable. The derivation of transport equations is standard. The evolution of particle number distributions is encoded in the time-ordered two-point correlation function. Its imaginary and real part is determined by the commutator and anti-commutator of two fields:

$$\rho(x, y) = i\langle[\Phi(x), \Phi(y)]\rangle, \quad F(x, y) = \frac{1}{2}\langle\{\Phi(x), \Phi(y)\}\rangle. \quad (3)$$

Here  $\rho(x, y)$  denotes the spectral function and  $F(x, y)$  the statistical two-point function. While the spectral function encodes the spectrum of the theory, the statistical propagator gives information about occupation numbers. Loosely speaking, the decomposition makes explicit what states are available and how they are occupied. For nonequilibrium  $F(x, y)$  and  $\rho(x, y)$  are in general two independent two-point functions, whose exact time evolution equation reads<sup>2</sup>

$$\begin{aligned} [\square_x + M^2(x)] F(x, y) &= -\int_0^{x^0} dz^0 \int_{-\infty}^{\infty} d^3z \Sigma_\rho(x, z) F(z, y) \\ &\quad + \int_0^{y^0} dz^0 \int_{-\infty}^{\infty} d^3z \Sigma_F(x, z) \rho(z, y), \end{aligned} \quad (4)$$

$$[\square_x + M^2(x)] \rho(x, y) = -\int_{y^0}^{x^0} dz^0 \int_{-\infty}^{\infty} d^3z \Sigma_\rho(x, z) \rho(z, y). \quad (5)$$

---

<sup>2</sup>For a detailed derivation see e.g. Ref. [6]. We are considering the equations for Gaussian initial conditions, which are underlying transport equations. More involved initial conditions can be considered using higher  $n$ -PI effective actions [6].

These are causal equations with characteristic “memory” integrals, which integrate over the time history of the evolution starting at time  $t_0 = 0$ . Since they are exact they are equivalent to any kind of identity for the two-point functions such as Schwinger-Dyson/Kadanoff-Baym equations. Here  $\Sigma_F(x, y)$  denotes the real part and  $-\Sigma_\rho(x, y)/2$  the imaginary part of the self-energy  $\Sigma$ , where the local contribution is taken into account in  $M^2(x)$ . In 2PI approximations the self-energy  $\Sigma$  is obtained from the two-particle irreducible effective action [ 7]. Here we consider a three-loop 2PI effective action [ 4]. It includes direct scatterings, off-shell and memory effects. Most importantly in this context, it employs no derivative expansion. The latter is a basic ingredient for transport or kinetic theory.

Transport equations are obtained from the exact equations by the following prescription:

1) The lower bound ( $t_0 = 0$ ) of the time-integrals in (4) is sent to the infinite past, i.e.  $t_0 \rightarrow -\infty$ . Of course, a system that thermalizes would have reached already equilibrium at any finite time if initialized in the remote past. Therefore, in practice a “hybrid” description is employed: transport equations are initialized by prescribing  $F$ ,  $\rho$  and derivatives at a *finite* time using the equations with  $t_0 \rightarrow -\infty$  as an approximate description.

2) Employ a gradient expansion. In practice, this expansion is carried out to lowest order (LO) or next-to-lowest order (NLO) in the number of derivatives with respect to the center coordinates  $X^\mu \equiv (x^\mu + y^\mu)/2$  and powers of the relative coordinates  $s^\mu \equiv x^\mu - y^\mu$ .

3) Even for finite  $X^0$  one assumes that the relative-time coordinate  $s^0$  ranges from  $-\infty$  to  $\infty$  in order to achieve a convenient description in Wigner space, i.e. in Fourier space with respect to the relative coordinates.

We emphasize that the *ad hoc* approximations 1) and 3) are in general not controlled by a small expansion parameter. They require a loss of information about the details of the initial state. More precisely, they can only be expected to be valid for sufficiently late times  $t$  when initial-time correlations become negligible, i.e.  $\langle \Phi(0, \vec{x}) \Phi(t, \vec{y}) \rangle \simeq 0$ . The standard approximations 1) and 3) may, in principle, be evaded. However, if they are not applied then a gradient expansion would become too cumbersome to be of use in practical calculations.

The NLO transport equations for  $\tilde{F}(X; p) = \int d^4s e^{ips} F(X + s/2, X - s/2)$  and  $\tilde{\varrho}(X; p) = -i \int d^4s e^{ips} \rho(X + s/2, X - s/2)$  in Wigner space are given by

$$\begin{aligned}
& [2p^\mu \partial_{X^\mu} + (\partial_{X^\mu} M^2(X)) \partial_{p_\mu}] \tilde{F}(X, p) = \tilde{\Sigma}_\varrho(X, p) \tilde{F}(X, p) - \tilde{\Sigma}_F(X, p) \tilde{\varrho}(X, p) \\
& \quad + \left\{ \tilde{\Sigma}_F(X, p), \text{Re} \tilde{G}_R(X, p) \right\}_{PB} + \left\{ \text{Re} \tilde{\Sigma}_R(X, p), \tilde{F}(X, p) \right\}_{PB}, \quad (6) \\
& [2p^\mu \partial_{X^\mu} + (\partial_{X^\mu} M^2(X)) \partial_{p_\mu}] \tilde{\varrho}(X, p) \\
& \quad = \left\{ \tilde{\Sigma}_\varrho(X, p), \text{Re} \tilde{G}_R(X, p) \right\}_{PB} + \left\{ \text{Re} \tilde{\Sigma}_R(X, p), \tilde{\varrho}(X, p) \right\}_{PB}, \quad (7)
\end{aligned}$$

where  $G_R(x, y) \equiv \Theta(x^0 - y^0) \rho(x, y)$  and  $\Sigma_R(x, y) \equiv \Theta(x^0 - y^0) \Sigma_\rho(x, y)$  denote the retarded propagator and self-energy, and  $\{\dots\}_{PB}$  are the Poisson brackets. The

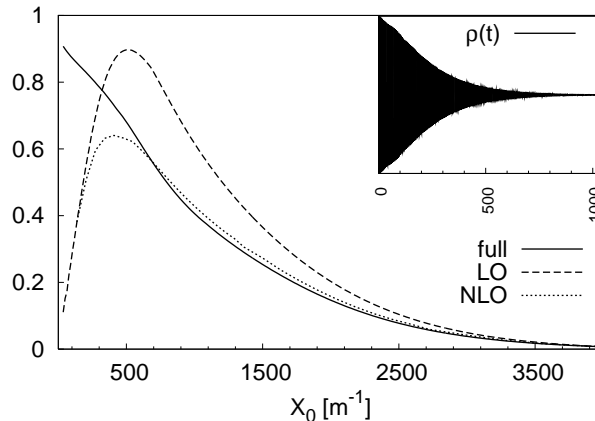


**Fig. 4.** Comparison of LO, NLO and full result for the on-shell  $2\omega\partial_{X^0}\tilde{F}$  with  $\lambda = 0.5$ . The LO transport equation fails to describe the full results until rather late times. Taking into account the substantial NLO corrections the gradient expansion becomes quite accurate for times larger than about  $t_{\text{damp}}$ .

corresponding LO equations are obtained by neglecting all contributions of order  $(\partial_{X^\mu}\partial_{p_\mu})^2$  in (6). The LO equations are typically used to obtain kinetic equations with the further assumption of a quasi-particle picture.

Fig. 4 shows the time evolution of the on-shell derivative  $2\omega\partial_{X^0}\tilde{F}$ . The thick curve represents the “full” result, which is obtained from solving the evolution equations (4) and (5) for the three-loop 2PI effective action. For comparison, we evaluate the same quantity using the LO gradient expansion according to Eq. (6). For this we evaluate the RHS of the LO terms in Eq. (6) using the full result for  $\tilde{F}$ . If the gradient expansion to lowest order is correct, then both results have to agree. Indeed, one finds that the curves for the LO (dashed) and the full result indeed agree at sufficiently late times. Taking into account the NLO contributions the agreement can be improved substantially. The NLO curve (dotted) in Fig. 4 approaches the full result rather closely, however, they only agree *after* some characteristic time. The latter is determined by the time scale  $\sim t_{\text{damp}}$  for the effective loss of details about the initial conditions. This can be observed, e.g., from the decay of the unequal-time two-point function shown in the inset. The latter measures correlations at time  $t$  with the initial state and its decay on the time scale  $\sim t_{\text{damp}}$  coincides rather well with the time for the onset of validity of the NLO result.

We have done a series of comparisons for various couplings in Ref. [4] and conclude that for times sufficiently large compared to  $t_{\text{damp}}$  the gradient expansion seems to converge well. There are sizeable NLO corrections already for couplings of about  $\lambda \simeq 1/4$ . Nevertheless, one observes that the NLO result can get rather close to the full result for  $\lambda \lesssim 1$  [4]. Times shorter than about  $t_{\text{damp}}$  seem clearly to be beyond the range of validity of transport equations even for weak couplings. This should make them unsuitable to discuss aspects of apparent early thermalization

and stresses the need to employ proper equations such as (4) and (5) for initial-value problems.

### 3. Beyond 2PI expansions: direct lattice simulations

We have seen above that the techniques based on two-particle or higher irreducible generating functionals are crucial for our analytical understanding of nonequilibrium quantum fields. However, analytical approaches necessarily involve approximations such as a 2PI loop expansion. Nonequilibrium approximations are difficult to test for crucial questions of QCD, i.e. where strong interactions can play an important role. Here direct numerical simulations of the quantum field theory on a space-time lattice, i.e. without truncations, could boost our knowledge and trigger the development of further approximate analytical tools.

Despite the importance of non-perturbative lattice simulation techniques in out-of-equilibrium quantum field theory, these are still in its infancies. This is in sharp contrast to well-established thermal equilibrium methods. Equilibrium calculations can typically be based on a Euclidean formulation, where the time variable is analytically continued to imaginary values. By this the quantum theory is mapped onto a statistical mechanics problem, which can be simulated by importance sampling techniques. Nonequilibrium problems, however, are not amenable to a Euclidean formulation. Moreover, for real times standard importance sampling is not possible because of a non-positive definite probability measure. A very interesting recent development employs stochastic quantization techniques for real times, which do not require a probability distribution [ 8]. Clearly, the possibility of direct simulations in nonequilibrium quantum field theory would mark a breakthrough not only for the description of QCD dynamics.

In Ref. [ 8] first lattice simulations of nonequilibrium quantum fields in Minkowski space-time have been presented. For the example of a scalar field theory with quartic self-interaction this was used to compute the time evolution of correlation functions and characteristic time scales. Starting from a non-thermal initial state, the real-time quantum ensemble in 3+1 dimensions is constructed by a stochastic process in an additional (5th) ‘‘Langevin-time’’ using the reformulation of stochastic quantization for the Minkowskian path integral [ 9]. In addition to the space-time variable  $x$  the field  $\phi$  depends on the Langevin-time parameter  $\vartheta$  with

$$\frac{\partial\phi}{\partial\vartheta} = i\frac{\delta S[\phi]}{\delta\phi} + \eta, \quad (8)$$

where  $S$  denotes the classical action and  $\eta$  Gaussian or white noise. For a real quantum field theory the Langevin dynamics governs a *complex*  $\phi = \phi_R + i\phi_I$ , where the appearance of an imaginary part reflects the fact that in the quantum theory the field picks up a phase by evolving in time.

The stochastic process (8) is associated to a real distribution  $P(\phi_R, \phi_I; \vartheta)$  and



averages of observables  $A(\phi)$  are given as area integrals in the complex field plane:

$$\langle A \rangle_\eta = \frac{\int [d\phi_R][d\phi_I] A(\phi_R + i\phi_I) P(\phi_R, \phi_I; \vartheta)}{\int [d\phi_R][d\phi_I] P(\phi_R, \phi_I; \vartheta)} \equiv \frac{\int [d\phi_R] A(\phi_R) P_{\text{eff}}(\phi_R; \vartheta)}{\int [d\phi_R] P_{\text{eff}}(\phi_R; \vartheta)}, \quad (9)$$

where the second equality defines the complex pseudo-distribution  $P_{\text{eff}}(\phi_R; \vartheta)$ . The latter is indeed governed by the analytic continuation of the Fokker-Planck equation to real times, which admits the stationary solution [ 9]

$$\lim_{\vartheta \rightarrow \infty} P_{\text{eff}}(\phi_R; \vartheta) \sim e^{iS[\phi_R]}. \quad (10)$$

Thus the approach can in principle be used for a Minkowskian theory, with “ensemble” averages calculated as averages along Langevin trajectories.

Some properties seem to make the approach quite suitable for out-of-equilibrium calculations. Firstly, nonequilibrium requires specification of an initial state or density matrix. Therefore, the initial configuration is fixed which seems to stabilize the procedure. Moreover, the additional averaging over an initial density matrix can help to achieve fast convergence. Secondly, one typically has a good guess for the 3 + 1 dimensional starting configurations of the Langevin updating procedure: In contrast to the quantum theory, the corresponding classical statistical field theory can be simulated using numerical integration and Monte Carlo techniques [ 6]. Using the nonequilibrium classical statistical solution as the starting configuration can improve convergence. Here the classical field configurations are obtained by numerically solving the classical field equation of motion and sampling over initial conditions, with nonzero field average and Gaussian fluctuations. It also provides a crucial check of the quantum result in some limiting cases: For sufficiently large macroscopic field or occupation numbers classical dynamics can provide a good approximation for the quantum evolution at not too late times [ 10].

Fig. 5 shows the time evolution for the connected part of the unequal-time correlator  $\text{Re}\langle \int_x \Phi(0, \vec{x}) \Phi(t, \vec{x}) \rangle$ , which measures the correlation of the field at time  $t$  with the initial field. It gives important information about the characteristic time scale for the loss of details about the initial conditions, as explained in Sec. 1.

One finds good convergence properties of the quantum simulations, which is a remarkable result. For given initial field configurations at time  $t = 0$ , very different starting configurations for the 3+1 dimensional space-time lattice converge to the same nonequilibrium dynamics for all  $t > 0$ . To obtain this one had to resolve the problem of possible unstable dynamics for the updating procedure [ 8]. Though more or less formal proofs of equivalence of the stochastic approach and the path integral formulation have been given for Minkowski space-time, not much is known about the general convergence properties and its reliability.

Two procedures can be employed for further tests of the algorithm. Firstly, one can compare to analytical approximations based on two-particle irreducible effective actions [ 11]. Secondly, going to sufficiently late times one can compare to certain thermal equilibrium results from Euclidean simulations.

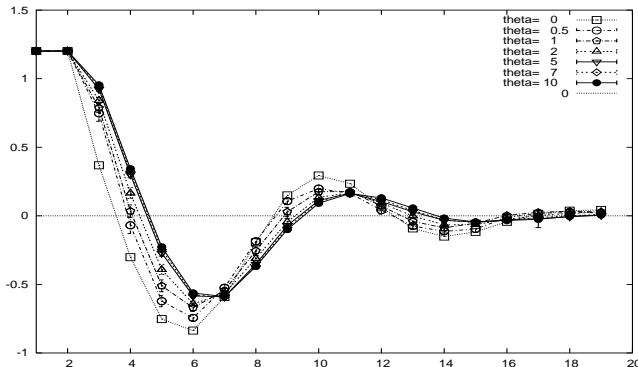


**Fig. 5.** The real part of  $\langle \int_x \Phi(0, \vec{x}) \Phi(t, \vec{x}) \rangle$  as a function of time  $t$  in units of the lattice spacing  $a$ . As starting configuration ( $\vartheta = 0$ ) the classical result is taken, and the Langevin updating ( $\vartheta > 0$ ) incorporates quantum corrections [ 8].

The range of potential applications of first-principles simulations in nonequilibrium quantum field theory is enormous. They may be used for out-of-equilibrium as well as Minkowskian equilibrium properties extracted at late times. Possible applications to QCD require implementation in a non-Abelian gauge theory, which is work in progress [ 11].

We thank Ion-Olimpiu Stamatescu and Christof Wetterich for very fruitful collaborations on recent related work.

## References

1. J. Berges, S. Borsanyi and C. Wetterich, Phys. Rev. Lett. **93** (2004) 142002.
2. P. Arnold, J. Lenaghan, G. D. Moore and L. G. Yaffe, Phys. Rev. Lett. **94** (2005) 072302.
3. U. W. Heinz, AIP Conf. Proc. **739** (2005) 163.
4. J. Berges, S. Borsanyi and C. Wetterich, Nucl. Phys. **B** to appear [arXiv:hep-ph/0505182]. J. Berges and S. Borsanyi, [arXiv:hep-ph/0512155].
5. S. Mrowczynski, Phys. Lett. B **314** (1993) 118; A. Rebhan, P. Romatschke and M. Strickland, Phys. Rev. Lett. **94** (2005) 102303.
6. J. Berges, AIP Conf. Proc. **739** (2005) 3 [arXiv:hep-ph/0409233], and references therein.
7. J. M. Cornwall, R. Jackiw and E. Tomboulis, Phys. Rev. D **10** (1974) 2428.
8. J. Berges and I. O. Stamatescu, Phys. Rev. Lett. **95** (2005) 202003.
9. G. Parisi and Y.-S. Wu, Sci. Sin. **24** (1981) 483. H. Hüffel and H. Rumpf, Phys. Lett. B **148** (1984) 104. P. H. Damgaard and H. Hüffel, Phys. Rept. **152** (1987) 227.
10. G. Aarts and J. Berges, Phys. Rev. Lett. **88** (2002) 041603.
11. J. Berges, S. Borsanyi and I. O. Stamatescu, work in progress.